SCIENCE CHINA Materials ARTICLES

mater.scichina.com link.springer.com

Published online 20 September 2019 | https://doi.org/10.1007/s40843-019-9587-5

Sci China Mater 2020, 63(2): 229–239

$NiCoSe_2/Ni_3Se_2$ lamella arrays grown on N-doped graphene nanotubes with ultrahigh-rate capability and long-term cycling for asymmetric supercapacitor

Alan Meng[1], Tong Shen[1], Tianqi Huang[1], Guanying Song[2], Zhenjiang Li[2], Shuqin Tan[3] and Jian Zhao[2*]

ABSTRACT **In this paper, we report a one-step electrodeposited synthesis strategy for directly growing $NiCoSe_2/Ni_3Se_2$ lamella arrays (LAs) on N-doped graphene nanotubes (N-GNTs) as advanced free-standing positive electrode for asymmetric supercapacitors. Benefiting from the synergetic contribution between the distinctive electroactive materials and the skeletons, the as-constructed N-GNTs@$NiCoSe_2/Ni_3Se_2$ LAs present a specific capacitance of ~1308 F g^{-1} at a current density of 1 A g^{-1}. More importantly, the hybrid electrode also reveals excellent rate capability (~1000 F g^{-1} even at 100 A g^{-1}) and appealing cycling performance (~103.2% of capacitance retention over 10,000 cycles). Furthermore, an asymmetric supercapacitor is fabricated by using the obtained N-GNTs@$NiCoSe_2/Ni_3Se_2$ LAs and active carbon (AC) as the positive and negative electrodes respectively, which holds a high energy density of 42.8 W h kg^{-1} at 2.6 kW kg^{-1}, and superior cycling stability of ~94.4% retention over 10,000 cycles. Accordingly, our fabrication technique and new insight herein can both widen design strategy of multicomponent composite electrode materials and promote the practical applications of the latest emerging transition metal selenides in next-generation high-performance supercapacitors.**

Keywords: $NiCoSe_2/Ni_3Se_2$ lamella arrays, electrodeposition, N-doped graphene nanotubes, rate capability, asymmetric supercapacitor

INTRODUCTION

With the significant increase in the consumption of portable electronic devices, electric vehicles and mobile phones, supercapacitors (SCs) have recently drawn much attention due to their ultrahigh power density, long-span cycle life, lightweight and environment friendliness [1–5]. The currently available SCs, although able to possess versatile features, only have an energy density that is one to two orders of magnitude lower than that of a typical rechargeable ion battery [6,7]. The electrode materials are the key components of SCs, which determine their electrochemical performances. A feasible approach to enhance the energy density of SCs is to harness reversible multielectron redox reactions in each redox center to increase the capacitive properties of the electrode materials [8]. Nickel cobalt compounds including hydroxides, oxides and sulfides as electrode materials can present much higher specific capacitance by providing more redox reactions. It is mainly ascribed to the contributions from both nickel and cobalt ions and their cooperative influences as compared to electrode materials with individual nickel or cobalt ions [9–11]. However, these electrode materials always encounter inferior cycling performance or weak rate capability, which can be attributed to their poor electronic conductivity and greatly limit their commercial attractiveness [12,13]. Thus, it is necessary to develop a new class of Ni/Co based electrode [14] materials with excellent electronic conductivity to meet the requirements of high-performance SCs.

As the neighbor of oxygen (O) and sulfur (S), selenium (Se) not only possesses the same valance electron and similar oxidation numbers as these two elements, leading

[1] Key Laboratory Base of Eco-chemical Engineering, College of Chemistry and Molecular Engineering, College of Materials Science and Engineering, Qingdao University of Science and Technology, Qingdao 266042, China
[2] Key Laboratory of Polymer Material Advanced Manufacturing Technology of Shandong Provincial, College of Electromechanical Engineering, College of Sino-German Science and Technology, Qingdao University of Science and Technology, Qingdao 266061, China
[3] Library, Qingdao University of Science and Technology, Qingdao 266042, China
* Corresponding author (email: zhaojian19880105@163.com)

to homologous electrochemical performance and ample chemical active sites, but also has a high electronic conductivity of ~1×10^{-3} S m^{-1}, which is much larger than that of S (0.5×10^{-27} S m^{-1}) at room temperature [15,16]. Thus, Ni/Co selenides, especially $NiCoSe_2$, have appeared as a novel family of electrode materials with attractive electrical conductivity, high theoretical specific capacitance, satisfied electrochemical activities, multifarious valences, as well as worldwide abundance and low cost for advanced SCs [1,8,17]. Additionally, Ni_3Se_2, a significant member of nickel selenide family, also possesses a superior charge transfer capability, excellent physical-chemical features and stable phase structures [18,19]. Therefore, as expected, a combination of $NiCoSe_2$ and Ni_3Se_2 as a novel hybrid composite can act as an ideal electrode material for SCs due to their synergistic effect. However, most of the approaches used in the previous reports [20–22] to develop hybrid selenide nanomaterials usually require multiple complicated steps including secondary ion-exchange or selenization procedures. It immensely restricts their productivity and makes it difficult for the active materials to grow on the conductive substrates *in situ*. In addition, there has been no direct and effective experimental data that has verified the good rate capability of Ni/Co selenides when the current density is enlarged to tens or even hundreds of times of the original value. Moreover, in general, nanoscale electrode structures can all easily aggregate on the substrate during the fabrication process, preventing the active materials from fully contacting the electrolyte. Thus, it is imperative to find a decent conductive skeleton on which to grow active materials using a one-step *in-situ* method to obtain evenly distributed products.

Recently, tubular graphene has been demonstrated to be a strong framework of hybrid electrode materials for various applications in energy storage and conversion scopes containing fuel cell [23], supercapacitors [24], and electrocatalyst [25] because it exhibits inner hollow channels, superior electrical conductivity, outstanding physicochemical stability, anticorrosion capability and satisfactory mechanical strength [26–29]. Moreover, a hollow skeleton with a larger diameter of about 150–200 nm can play a role of an efficient "ion reservoir", effectively providing the continuous supply of OH^- ions and an available diffusion path. Moreover, N-doping is one of the most efficient methods for enhancing the electrical conductivity of electrode materials [30,31]. Based on the preceding analysis, high-performance electrode materials for SCs can be achieved by using N-doped graphene nanotubes (N-GNTs) as supporters and employing a one-step direct preparation approach for growing $NiCoSe_2/Ni_3Se_2$ on the skeletons to form a composite.

Herein, we design advanced hybrid electrode nanostructures that are composed of N-GNT skeletons with aligned sheet-like $NiCoSe_2/Ni_3Se_2$ active materials prepared *via* a one-step electrodeposition process. Benefiting from their synthetic strategy, the N-GNTs@$NiCoSe_2/Ni_3Se_2$ not only displays satisfactory specific capacitance, but also exhibits ultrahigh rate capability and long-term cycling performance. In addition, the fabricated nanoarchitectures and activated carbon (AC) as positive and negative electrode materials are respectively selected to assemble an asymmetric supercapacitor (ASC) device, which also demonstrates excellent energy/power density. Thus, the construction route greatly promotes the emerging Ni/Co selenides in energy storage applications.

EXPERIMENTAL SECTION

Chemicals and materials

Nickel chloride hexahydrate ($NiCl_2\cdot6H_2O$), cobalt chloride hexahydrate ($CoCl_2\cdot6H_2O$), selenium dioxide (SeO_2), lithium chloride (LiCl) and potassium hydroxide (KOH) were purchased from Sinopharm Chemical Reagent Co., Ltd. All the chemical reagents were AR grade and used without further purification treatment.

Preparation of N-GNTs

The synthesis of N-GNTs was performed by chemical vapor reactions (CVR) in a traditional high-temperature vacuum furnace. The specific experimental processes could be found in our previous literatures [24,32].

Fabrication of the N-GNTs@$NiCoSe_2/Ni_3Se_2$ LAs electrode materials

The $NiCoSe_2/Ni_3Se_2$ LAs were achieved through one-step eletrodeposition procedure using a graphite substrate (1×1 cm^2) deposited with N-GNTs as working electrode, an Pt wire counter electrode and a saturated calomel reference electrode in a hybrid electrolyte solution of 17 mmol L^{-1} $NiCl_2\cdot6H_2O$, 3 mmol L^{-1} $CoCl_2\cdot6H_2O$, 20 mmol L^{-1} SeO_2 and 0.1 mol L^{-1} LiCl at the electrodeposition potential of −0.8 V for 600 s. After electrodeposition, the samples were rinsed with deionized (DI) water and ethanol several times, and dried at 60°C for 12 h. The obtained product is N-GNTs@$NiCoSe_2/Ni_3Se_2$ LAs (marked as N-GNTs@Ni-Co-Se-M). In contrast, the bare $NiCoSe_2/Ni_3Se_2$ LAs (Ni-Co-Se-M) were directly fabricated on a graphite substrate in the same manner

under the same conditions. What's more, the control samples of N-GNTs@Ni-Co-Se-L and N-GNTs@Ni-Co-Se-H were also synthesized in the same manner under the same conditions except the molar ratios of the Ni^{2+} and Co^{2+} in the solution were 19:1 and 15:5, respectively. The typical mass loading of the N-GNTs@Ni-Co-Se-L, N-GNTs@Ni-Co-Se-M, N-GNTs@Ni-Co-Se-H, and Ni-Co-Se-M were about 0.7, 0.6, 0.7, and 0.6 mg cm^{-2}, respectively.

Assembly of asymmetric supercapacitor

An AC electrode was prepared *via* mixing AC, polyvinylidenedifluoride (PVDF) and carbon black (weight ratio of 80:10:10) in *N*-methyl-2-pyrrolidinone (NMP) and then spread onto a nickel foam (NF). This negative electrode was then pressed and coupled with the N-GNTs@Ni-Co-Se-M hybrid positive electrode with 2 mol L^{-1} KOH as the electrolyte and filter paper as separator to assemble an ASC device. The typical mass loading of the AC electrode materials was 2.3 mg cm^{-2}, which was confirmed according to the well-known charge balance theory [33]. Thus, the mass ratio of anode to cathode was ~3.83.

Characterizations

The morphology and chemical elements were investigated by utilizing a JEOL JSM-6 field emission scanning electron microscope (FESEM). Further specific structural information was obtained by employing a Hitachi (Tokyo, Japan) H-8100 transmission electron microscope (TEM) and high resolution TEM (HRTEM). The X-ray powder diffraction (XRD) patterns of the product were recorded by using an Advance D8 X-ray diffractometer. Additionally, X-ray photoelectron spectroscopy (XPS) characterization was carried out to further analyze the elemental valence states and chemical compositions on a Thermo ESCALAB 250Xi device with an Al-Kα ($h\nu$= 1486.6 eV) excitation source.

Electrochemical measurements

The electrochemical performances of the single electrode were tested in a standard three-electrode system. The as-prepared electrode materials were selected as the working electrode, with Pt wire as the counter electrode and an Hg/HgO as reference electrode. The electrochemical analysis of the assembled device was conducted in a two-electrode configuration. The electrochemical measurements such as cyclic voltammetry (CV), galvanostatic charge-discharge (GCD) as well as electrochemical impedance spectroscopy (EIS) were performed on an electrochemical workstation (CHI 660E, Shanghai Chenhua Instrument Co., Shanghai, China) at room temperature with 2 mol L^{-1} KOH as the electrolyte.

RESULTS AND DISCUSSION

N-GNTs@$NiCoSe_2$/Ni_3Se_2 electrode materials on graphite substrate were prepared using one-step electrodeposition, and the synthetic procedure and preparation mechanisms illustrated in Fig. 1, are expressed as follows [34]:

$$SeO_2 + H_2O \rightarrow H_2SeO_3, \quad (1)$$

$$H_2SeO_3 + 4H^+ + 4e^- \rightarrow Se + 3H_2O, \quad (2)$$

$$Se + 2e^- \rightarrow Se^{2-}, \quad (3)$$

$$Ni^{2+} + Co^{2+} + 2Se^{2-} \rightarrow NiCoSe_2. \quad (4)$$

Owing to the excessive amount of additives in the Ni resource, redundant Ni ions can couple with Se^{2-} to achieve Ni_3Se_2 and $NiCoSe_2$ [35]. The as-synthesized products are thus composed of $NiCoSe_2$/Ni_3Se_2 hybrids on the N-GNTs (denoted as N-GNTs@Ni-Co-Se-M).

Fig. 2a–c present the typical microscopic characteristics of the N-GNTs. As shown in Fig. 2a, b (SEM images at different magnifications), the obtained N-GNTs are several microns long and have smooth surfaces grown on the graphite substrate to form densely-packed conductive networks over a large area with excellent homogeneity. Moreover, EDS inset in Fig. 2b clearly shows the elements C and N well distributed throughout the tube-like region. Fig. 2c presents the TEM image of the N-GNTs, and the diameter of the nanotube with smooth surface is evidently larger, about 150–200 nm. A corresponding

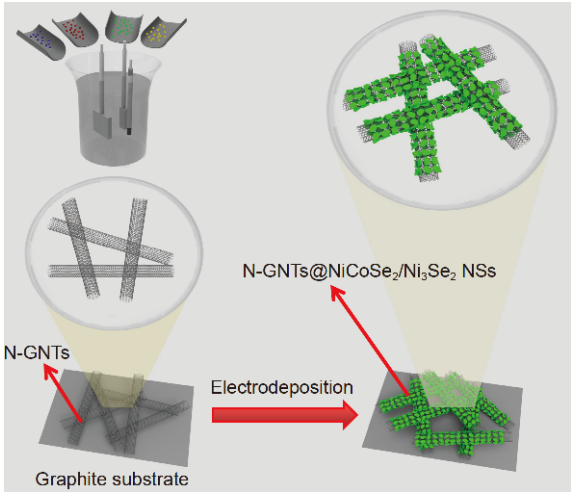

Figure 1 Schematic diagram of the fabrication of N-GNTs@$NiCoSe_2$/Ni_3Se_2 NSs electrode materials.

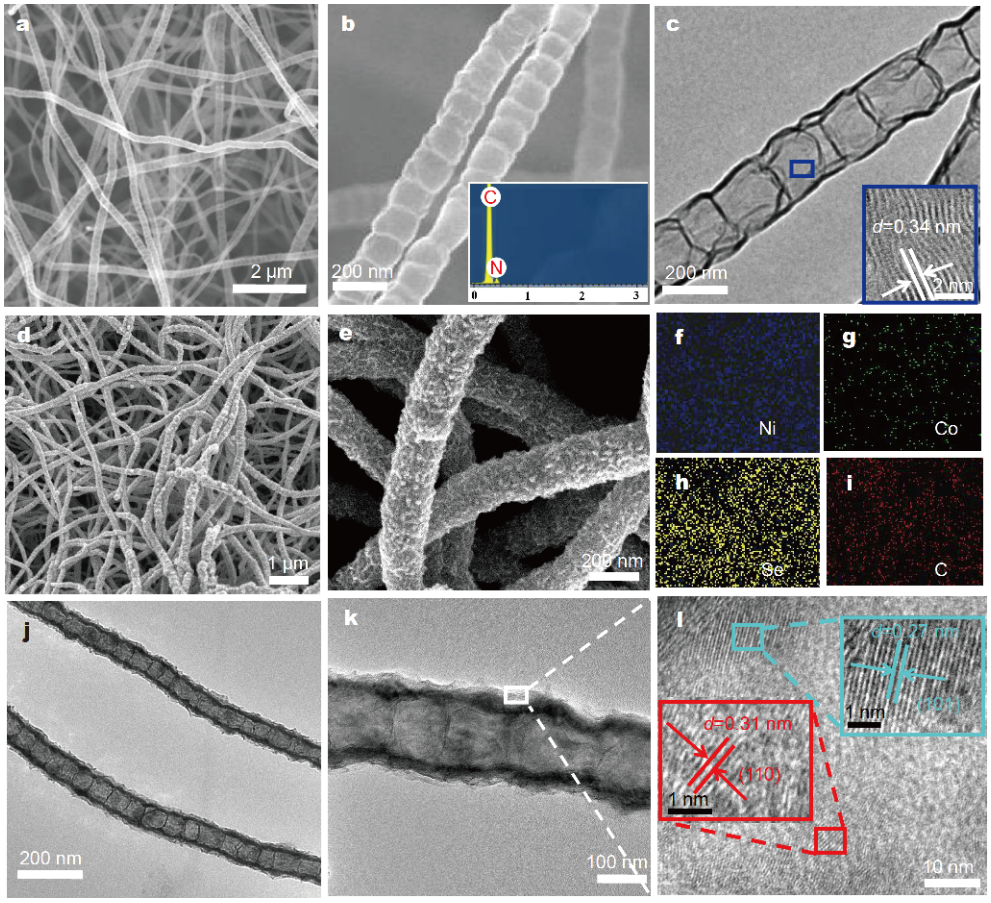

Figure 2 SEM images (a, b) and TEM image (c) of the N-GNTs. The inset in (b) is the corresponding EDS spectrum, and the inset in (c) depicts the HRTEM plot. Low-magnification (d) and high-magnification (e) SEM images of N-GNTs@Ni-Co-Se-M, and the corresponding elemental mapping images (f–i) of Ni, Co, Se and C; TEM images (j, k) and HRTEM image (l) of the sample.

HRTEM image (inset, Fig. 2c) reveals the highly crystalline nature of the nanotube, and an interplanar distance of 0.34 nm, which corresponds to the (002) plane of the graphite. To confirm the ratio of N-doping in the N-GNTs, XPS measurement of the as-fabricated N-GNTs was conducted. The corresponding high-resolution N 1s spectrum and detailed elemental composition are presented in Fig. S1 and Table S1, respectively. On the basis of the results, the N atoms were successfully incorporated into the graphene lattice, indicating that N–C bonds exist in the tube-like graphene. The atomic percentage of the N element is ~2.05%. The Raman characterization reported in our previous study [24,32] demonstrated that the samples were N-GNTs. Fig. 2d–l show the morphology and microstructure of the optimized N-GNTs@Ni-Co-Se-M core-branch heterojunction nanoarchitectures, as revealed by SEM, TEM, and HRTEM. After the deposition of high-density and neatly arranged Ni–Co selenides LAs deposited on the N-GNTs *via* electrodeposition, thinner layers and rougher surfaces are generated, and the homogeneous network architecture is remained as depicted in Fig. 2d. Meanwhile, the magnified SEM image (Fig. 2e) reveals that the uniform growth of a large amount of the active materials on the N-GNTs produces a typical branched core–shell heterojunction nanostructures. A broadly open void is found between adjacent nanosheets, which is conducive to greatly increasing the contact area between the active materials and the electrolyte. Such an increase allows more lamellas to participate in electrochemical reactions and thus improve their capacitive properties. Moreover, the chemical components of the fabricated product are distinguished by elemental mapping. As clearly observed in Fig. 2f–i and Fig. S2, Ni, Co, Se, and C are evenly dispersed throughout the full core-shell region. To distinguish the prepared products containing Ni_3Se_2, their EDS spectrum was obtained, and the corresponding chemical components were analyzed (Fig. S3). This analysis confirms that the pro-

ducts consist of the elements C, Co, Ni, and Se. Moreover, the atomic percentage of Co is 4.22%, namely the atomic percentage of Ni and Se in $NiCoSe_2$ is 4.22% and 8.44% respectively. Thus, atomic percentage of the redundant Ni and Se is 6.09% and 4.3% (the atomic ratio of Ni/Se is ~3:2), matching well with the formula of Ni_3Se_2. On the basis of the aforementioned analysis, the as-prepared products are verified to contain $NiCoSe_2$ and Ni_3Se_2. The TEM images of the obtained products in Fig. 2j, k clearly show that the surface of the N-GNTs supporters are almost entirely covered by numerous branched Ni–Co selenides LAs with a thickness of ~20 nm, gaining a typical branched core–shell heterostructured configuration. Such a firm contact at the interface between the active materials and the skeleton may contribute to accelerating electron transfer, consequently enhancing performances. The HRTEM image (Fig. 2l) of the shell exhibits clear fringes with a measured interplanar spacing of 0.27 and 0.31 nm assigning to the interplanar distance of the $NiCoSe_2$ (101) and Ni_3Se_2 (110) planes. On the basis of the aforementioned results, the synthesized products are determined as N-GNTs@Ni-Co-Se-M hybrid electrode materials.

XRD was performed to verify the phase information of the prepared N-GNTs@Ni-Co-Se-M. The results are displayed in Fig. 3a. The diffraction peaks of N-GNTs clearly appear at 26.5°. A set of diffraction peaks located at 32.9°, 44.5° and 50.4° are assigned to the (101), (102), and (110) planes of $NiCoSe_2$ (JCPDS No. 65-7038). Another series of diffraction peaks emerge at 29.5°, 42.3°, 52.6°, and 53.5°, corresponding to the (110), (002), (202), (122), and (104) planes of Ni_3Se_2 (JCPDS No. 19-0841). The different valence states and chemical composition of the as-synthesized product were further detected by XPS. The results are shown in Fig. S4 (survey spectrum), revealing the peaks of Ni 2p, Co 2p, and C 1s could be clearly observed. With regard to the Ni 2p spectrum (Fig. 3b), the expected Ni $2p_{3/2}$ (~855.4 eV) and Ni $2p_{1/2}$ (~873.0 eV) signals, along with the two satellites peaks at ~860.9 and ~879.1 eV, typically indicate the Ni^{2+} species from the $NiCoSe_2/Ni_3Se_2$ [1,36]. The Co 2p spectrum presented in Fig. 3c reveals that it can be deconvoluted into two spin-orbit doublets and two shakeup satellites. The two main peaks at 781.1 and 796.3 eV are ascribed to Co $2p_{3/2}$ and Co $2p_{1/2}$, respectively, which are the striking characteristics of the Co^{2+} signal in $NiCoSe_2$ [1]. In ad-

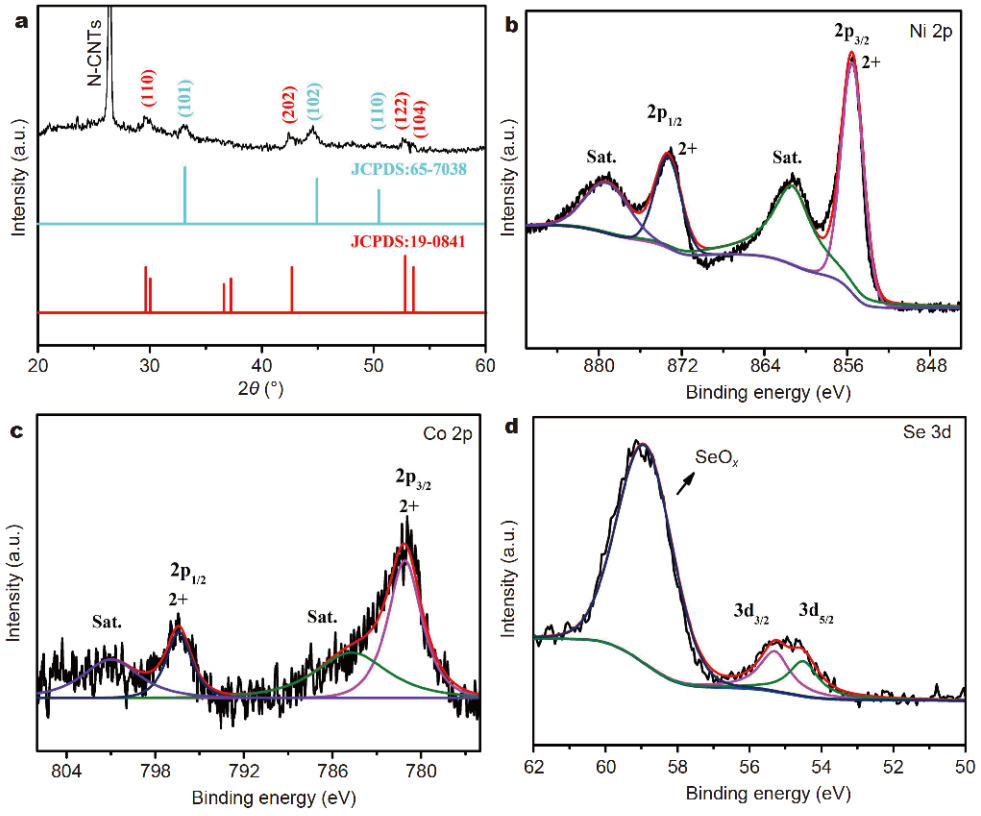

Figure 3 XRD pattern (a), and XPS high-resolution spectra of Ni 2p (b), Co 2p (c) and Se 3d (d) of the N-GNTs@Ni-Co-Se-M.

dition, the Se 3d spectrum (Fig. 3d) is deconvoluted into two peaks appearing at 54.6 and 55.5 eV, consistent well with Se $3d_{5/2}$ and Se $3d_{3/2}$, respectively, which signifies the presence of Se^{2-}. The existence of the SeO_x peak (58.6 eV) may be attributed to the surface oxidation of the selenide [37]. Therefore, the characterization results fully verify the successful growth of the materials.

The energy storage performances of these as-prepared electrodes were investigated *via* three-electrode configuration, as shown in Fig. 4. Fig. 4a presents the comparative CV plots of N-GNTs, N-GNTs@Ni-Co-Se-L, N-GNTs@Ni-Co-Se-M, N-GNTs@Ni-Co-Se-H, and Ni-Co-Se-M at the same scan rate of 20 mV s^{-1}. Notably, the N-GNTs@Ni-Co-Se-M electrode has a larger CV integrated area than those of other electrodes. This difference reveals that higher capacitance can be achieved using the hybrid electrode. Moreover, the CV curve of the sample delivers a pair of redox peaks, confirming the battery-type reversible faradaic behaviors based on the following redox reactions [18,22]:

$$NiCoSe_2 + 2OH^- \leftrightarrow CoSeOH + NiSeOH + 2e^-, \quad (5)$$

$$CoSeOH + OH^- \leftrightarrow CoSeO + H_2O + e^-, \quad (6)$$

$$NiSeOH + OH^- \leftrightarrow NiSeO + H_2O + e^-, \quad (7)$$

$$Ni_3Se_2 + 3OH^- \leftrightarrow Ni_3Se_2(OH)_3 + 3e^-. \quad (8)$$

Fig. 4b illustrates the GCD plots of the achieved electrodes at a constant current density of 1 A g^{-1}. All the GCD curves show a typical discharge platform because of the faradaic redox reactions, as expected, and the discharging time of the N-GNTs@Ni-Co-Se-M is considerably longer than those of the other electrodes. Accordingly, the N-GNTs@Ni-Co-Se-M delivers the largest specific capacitance among the electrodes. This finding coincides with the aforementioned CV analysis. Fig. 4c depicts the CV curves of the N-GNTs@Ni-Co-Se-M electrode at 5–50 mV s^{-1}. With an increase in the scan rates, the redox current intensity also increases and almost homologous CV plot shapes can be maintained. Meanwhile, the oxidation/reduction peaks slightly migrate toward higher and lower potentials, indicating the ideal conductive behavior and prominent rate property of the electrode. The specific capacities of these electrodes are evaluated using the corresponding GCD plots at 1–100 A g^{-1} (in Fig. 4d and Fig. S5) and the equation $Q = It_d/m$, where I is the discharge current, t_d refers to the discharge time, and m represents the mass of the electrode. The results were calculated from the curves presented in Fig. 4e. When the current density is smaller (1 A g^{-1}), the N-GNTs@Ni-Co-Se-M electrode can exhibit a high specific capacity of 181.7 mA h g^{-1}; however, the N-GNTs@Ni-Co-Se-L, N-GNTs@Ni-Co-Se-H, and Ni-Co-Se-M electrodes only deliver 112.9, 88.8, and 100.4 mA h g^{-1}, respectively. More importantly, when the current density is increased up to 100 A g^{-1}, the N-GNTs@Ni-Co-Se-M electrode still remains its superior rate capability (~76.5% capacitance retention of the initial value) relative to those of the other three electrodes (~12.3%, 28.2%, and 69% capacitance retention, respectively). Moreover, in accordance with the equation in the Supplementary information, the N-GNTs@Ni-Co-Se-M hybrid electrode can also present high specific capacitance of ~1308 F g^{-1} (at 1 A g^{-1}), and deliver 1000 F g^{-1} when the current density is increased to 100 A g^{-1} (Fig. S6). This finding indicates that the hybrid electrode has more advantages with respect to specific capacitance and rate capability than many other transition metal compounds reported in the literature in recent years, as shown in Table S2. EIS test was also carried out to explore the conductivity of these electrodes, as presented in Fig. 4f. The N-GNTs@Ni-Co-Se-M electrode shows lower internal resistance (0.69 Ω) than those of the other electrodes. Meanwhile, almost no charge transfer resistance is observed in the N-GNTs@Ni-Co-Se-M electrode. At a low frequency region, the line is nearly parallel to the imaginary axis, suggesting that it also exhibits satisfied diffusion resistance. Thus, the measurement results verify that the N-GNTs@Ni-Co-Se-M electrode displays outstanding conductivity, fast electron transfer kinetics, as well as easy ion diffusion at the interfaces of the electrode materials and the aqueous electrolyte. Another indispensable parameter that determines the practical application of these electrodes is long-term stability, which is measured by repeating GCD cycles at 20 A g^{-1} (Fig. 4g). After 10,000 cycles, the specific capacitance of the N-GNTs@Ni-Co-Se-M electrode shows no decay (~103.2% of the initial capacitance), confirming that the electrode materials exhibit excellent stability. By contrast, the specific capacitance retention rates of the N-GNTs@Ni-Co-Se-L, N-GNTs@Ni-Co-Se-H, and Ni-Co-Se-M electrodes are only 66.6%, 77.7% and 78.6%, respectively over 10,000 cycles. Moreover, the coulombic efficiency of all samples are approximately 100% over 10,000 cycles, presenting excellent reversibility during charging/discharging process (Fig. S7). Notably, the cycling performance of the hybrid electrode is better than that of the previously reported similar electrode materials presented in Table S3. To summarize, the N-GNTs@Ni-Co-Se-M electrode exhibits significant application potential in high-energy supercapacitor devices.

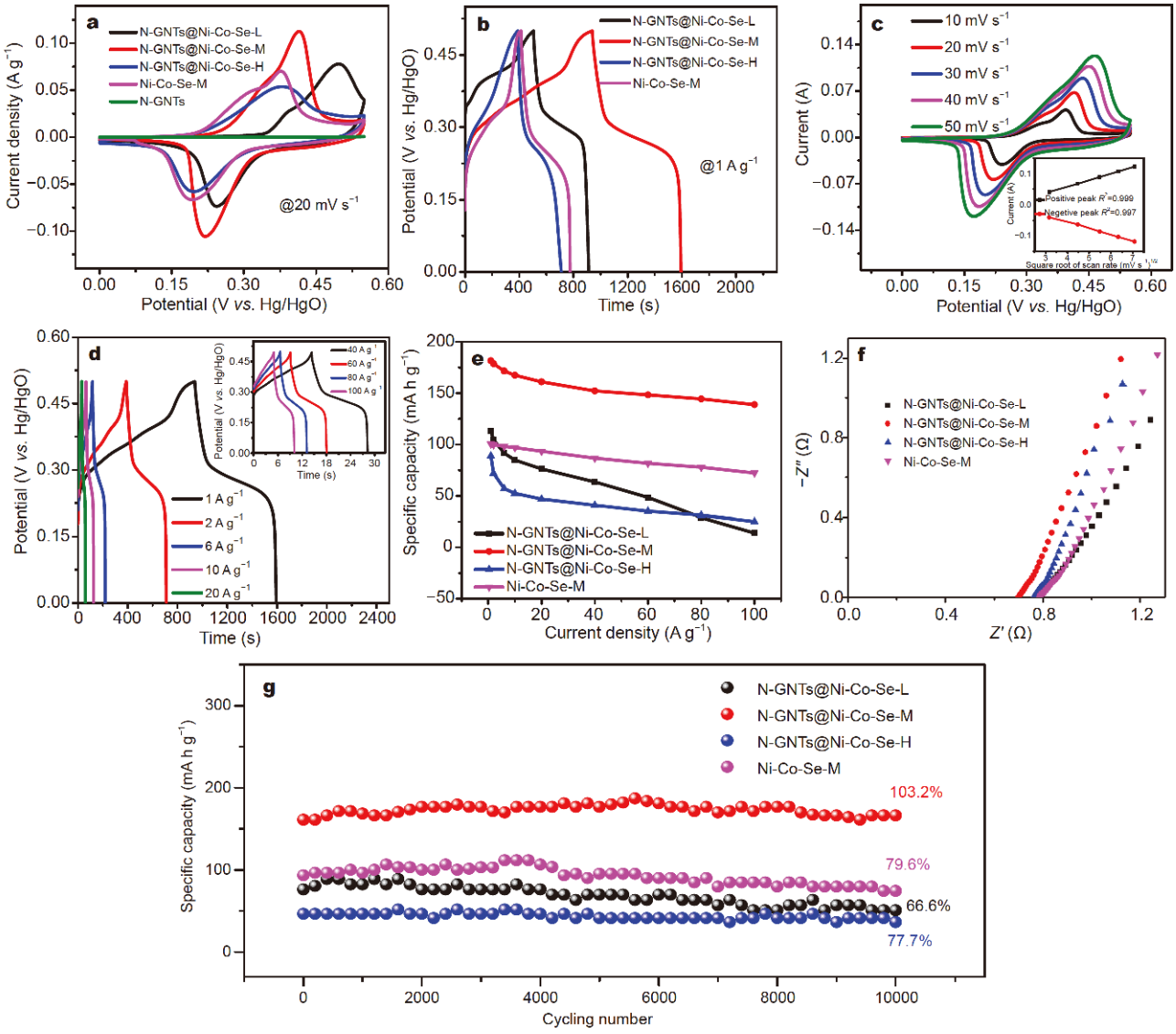

Figure 4 Comparative CV (a) and GCD (b) curves of these obtained electrodes at 20 mV s^{-1} and 1 A g^{-1} respectively. CV curves (c) of the N-GNTs@Ni-Co-Se-M electrode at different scan rates. GCD curves (d) of the N-GNTs@Ni-Co-Se-M electrode at various current densities. (e) Specific capacity *versus* current densities. EIS profiles (f) of these obtained electrodes. Cycling property (g) of these obtained electrodes at 20 A g^{-1} for 10,000 cycles.

The favorable electrochemical features of the hybrid electrode materials are attributed to the cooperative effects, as explained in the following: (1) the N-GNTs skeleton arbitrarily intersect to form a typical conductive network. This network provides sufficient electron transport channels and enables the Ni-Co-Se-M nanosheets to disperse evenly, leading to the optimal use of the active materials. The N-GNTs with numerous spaces can also act as a mechanical buffer, which effectively eliminates stress and regulates the volume change in the composite caused by the redox reactions. Therefore, it prevents the electrochemical corrosion and structural collapse of the hybrids simultaneously, considerably enhancing their long-term cycling performance. (2) The hollow N-GNT has a larger diameter, which supports its function as an "ion reservoir", ensuring the consecutive supply of the OH^- for prompt contact with the internal part of the active materials. (3) The Ni-Co-Se-M active materials with multicomponent features can endow more redox reactions. In addition, several free gaps exist between neighbouring nanosheets, resulting in ample electroactive sites. (4) Compared with those of O or S atom,

Se has a larger atomic radius and poorer adhesion with metals, causing prominent electric conductivity and higher activity. Thus, the synthesized metal selenides possess excellent electrical conductivity. The N-GNTs supporters also exhibit ideal electrical conductivity, which can be conducive to rapid electron transmission, significantly improving their rate capability. (5) The active materials are directly grown on the surfaces of the N-GNTs, and the supporters are directly deposited on the graphite substrate, effectively ensuring close bonding and significantly facilitating electron transfer. Based on the aforementioned analysis, the hybrid electrode materials can exhibit high specific capacitance. More significantly, they possess superior rate capability and long-term cycling stability.

To further investigate the actual application of the N-GNTs@Ni-Co-Se-M electrode, an ASC was constructed using the N-GNTs@Ni-Co-Se-M as the positive electrode and AC as the negative electrode in a 2 mol L^{-1} KOH electrolyte. The corresponding assembly diagram is shown in Fig. 5a. The AC negative electrode materials can exhibit good electrochemical properties (Fig. S8). The opposite potential window of the two electrodes shown in Fig. 5b indicates that the fabricated ASC device can po-

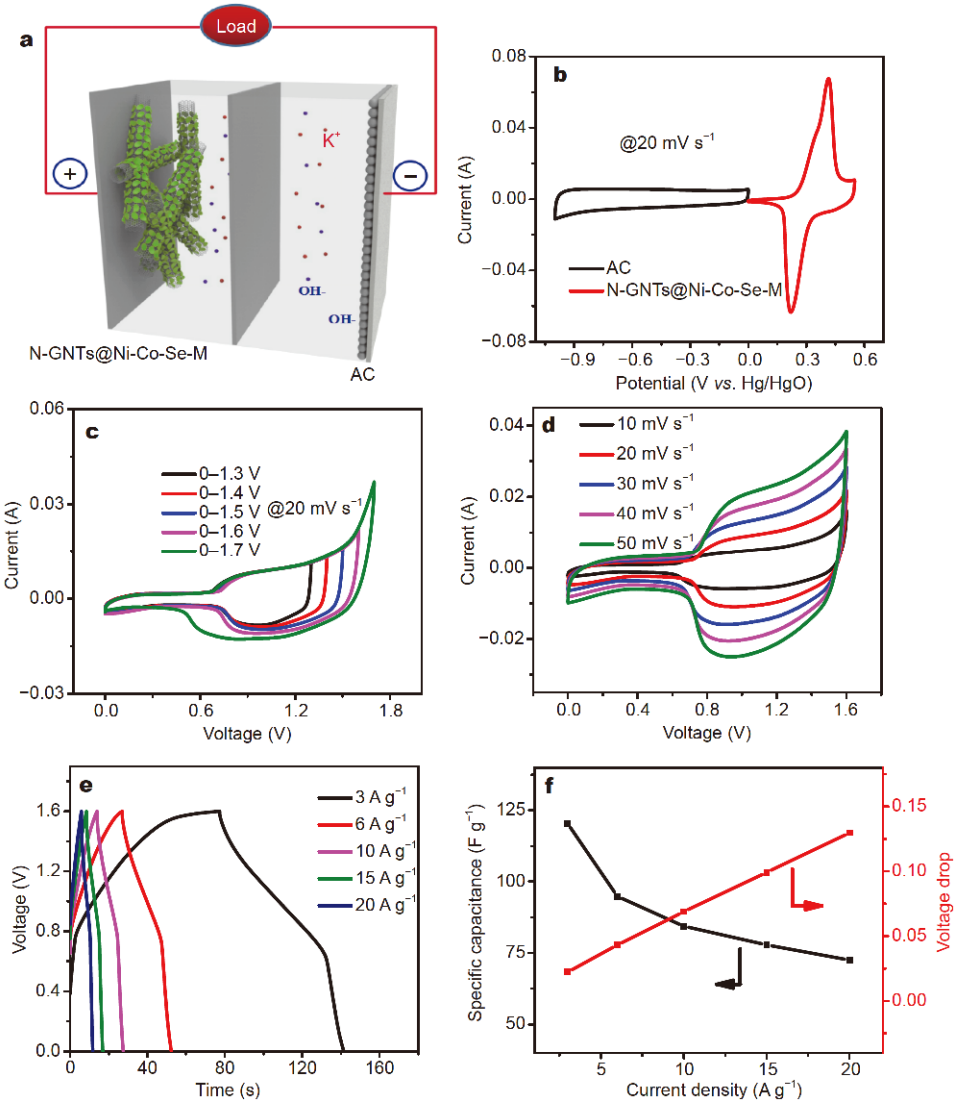

Figure 5 (a) A schematic diagram of the device assembly. (b) CV curves of N-GNTs@Ni-Co-Se-M and AC at 20 mV s^{-1}. (c) CV curves of various voltage windows. (d) CV plots at different scan rates. (e) GCD plots at different current densities of the ASC device. (f) Specific capacitance and voltage drop *vs.* current densities of the ASC device.

tentially obtain a higher operating voltage. To further determine the optimal voltage, the device was subjected to CV at the scan rate of 20 mV s^{-1} in various voltage windows (Fig. 5c). The device possesses a stable voltage window of 1.6 V. Fig. 5d presents the CV curves of the device at various scan rates of 10–50 mV s^{-1} within 0–1.6 V. The shapes of these CV plots are well-maintained even at a high scan rate of 50 mV s^{-1}, revealing a rapid current–voltage response and good electrochemical performances. The GCD curves of the device at different current densities are also shown in Fig. 5e. On the basis of the GCD curves and an equation in the Supplementary information, the corresponding specific capacitance are ~120, 94.8, 84.3, 77.8, and 72.5 F g^{-1} at 3, 6, 10, 15, and 20 A g^{-1}, respectively (Fig. 5f). Moreover, the ASC device confirms a small voltage drop even at a high current density. This finding suggests its low resistance and robust power as supported by the Nyquist plot generated in Fig. S9. As can be observed, the assembled device can potentially exhibit ideal electrical conductivity.

Fig. 6a shows the energy density and power density of the N-GNTs@Ni-Co-Se-M||AC ASC. The energy density of the device reaches 42.8 W h kg^{-1} at a power density of 2.4 kW kg^{-1}, calculated using the equation in the Supplementary information. When the power density reaches 16 kW kg^{-1}, the energy density of the device remains at 25.8 W h kg^{-1}. The maximum energy density obtained outperforms those of other ASCs reported previously, such as H-$NiCoSe_2$||AC (35.5 W h kg^{-1} at 0.188 kW kg^{-1}) [1], $Co(OH)_2$/NCNCs||AC (33 W h kg^{-1} at 0.8 kW kg^{-1}) [38], Ni_3S_2@CoS||AC (28.24 W h kg^{-1} at 134.46 W kg^{-1}) [39], $CoNi_2S_4$||AC (33.9 W h kg^{-1} at 409 W kg^{-1}) [40], Ni_3S_2-Co_9S_8/NF||AC (17 W h kg^{-1} at 1.1 kW kg^{-1}) [41], CNTF@$Co(OH)_2$||CNTF (13.03 W h kg^{-1} at 7.2 kW kg^{-1}) [42], MoS_2||AC (20.42 W h kg^{-1} at 750.31 W kg^{-1}) [43], Co_3O_4/$Co(OH)_2$||AC (25.6 W h kg^{-1} at 939 W kg^{-1}) [44]. Moreover, to visualize the practical application of the device, two ASCs were connected in series triggering an LED light and electric fan (Fig. 6b). The cycle life measurement of the N-GNTs@Ni-Co-Se-M||AC ASC at 8 A g^{-1} (Fig. 6c) demonstrates that the specific capacitance can be preserved at 94.4% after repeating a charge/discharge cycle 10,000 times. The inset in Fig. 6c displays the first 10 cycles and the last 10 cycles, which reveals that the GCD curves of the device are almost symmetric, confirming the favorable coulombic efficiency. These test

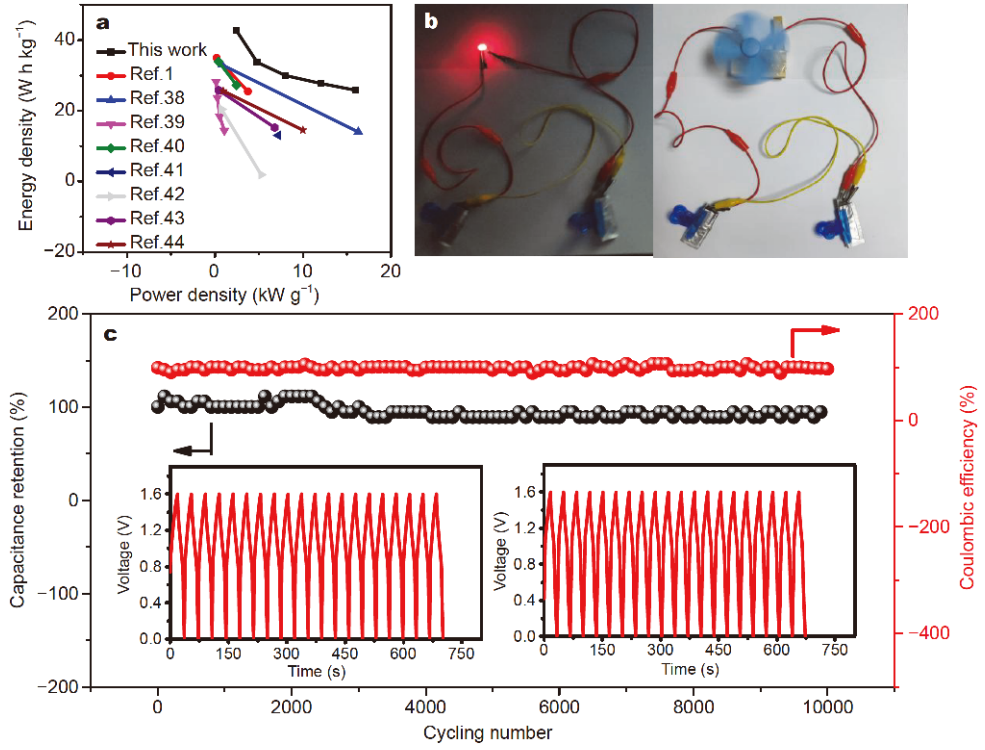

Figure 6 (a) Ragone profile (energy density *vs.* power density) of the assembled ASC device, and the comparison of the energy density between this work and the previous published reports. (b) Optical photograph of two ASC devices connected in series to power various electronic devices. (c) Cycling stability and corresponding coulombic efficiency of the ASC device. The inset displaying the first and last 20 cycles.

results confirm that the assembled device exhibits prominent cycle stability, and it is superior to that of the other many ASC devices widely studied in previous reports (Table S4).

CONCLUSIONS

In summary, we use an effective one-step *in-situ* electrodeposition to construct N-GNTs@$NiCoSe_2$/Ni_3Se_2 positive electrode materials with a typical core–branch nanostructure for ASCs. The rationally constructed hybrid electrode exhibits a satisfactory specific capacitance of 1308 F g^{-1} at 1 A g^{-1}, superior rate capability (~76.5% capacitance retention even at 100 A g^{-1}) and excellent cycling property (~103.2% capacitance retention over 10,000 cycles). These advantages are attributed to the synergy of the skeleton and the active materials. Furthermore, the achieved ASC device can also exhibit high energy density of 42.8 W h kg^{-1} at 2.4 kW kg^{-1} and superior cycling stability of 94.4% retention after 10,000 cycles at 8 A g^{-1}, which indicates its practical applicability in high-performance energy storage systems.

Received 18 July 2019; accepted 19 August 2019; published online 20 September 2019

1 Hou L, Shi Y, Wu C, *et al.* Monodisperse metallic $NiCoSe_2$ hollow sub-microspheres: Formation process, intrinsic charge-storage mechanism, and appealing pseudocapacitance as highly conductive electrode for electrochemical supercapacitors. Adv Funct Mater, 2018, 28: 1705921
2 Li X, Wu H, Elshahawy AM, *et al.* Cactus-like NiCoP/NiCo-OH 3D architecture with tunable composition for high-performance electrochemical capacitors. Adv Funct Mater, 2018, 28: 1800036
3 Wang HX, Zhang W, Drewett NE, *et al.* Unifying miscellaneous performance criteria for a prototype supercapacitor *via* $Co(OH)_2$ active material and current collector interactions. J Microsc, 2017, 267: 34–48
4 Wang H, Wang D, Deng T, *et al.* Insight into graphene/hydroxide compositing mechanism for remarkably enhanced capacity. J Power Sources, 2018, 399: 238–245
5 Oyedotun KO, Madito MJ, Momodu DY, *et al.* Synthesis of ternary NiCo-MnO_2 nanocomposite and its application as a novel high energy supercapattery device. Chem Eng J, 2018, 335: 416–433
6 Huang J, Peng Z, Xiao Y, *et al.* Hierarchical nanosheets/walls structured carbon-coated porous vanadium nitride anodes enable wide-voltage-window aqueous asymmetric supercapacitors with high energy density. Adv Sci, 2019, 6: 1900550
7 Gao X, Liu X, Wu D, *et al.* Significant role of Al in ternary layered double hydroxides for enhancing electrochemical performance of flexible asymmetric supercapacitor. Adv Funct Mater, 2019, 29: 1903879
8 Li X, Wu H, Guan C, *et al.* (Ni,Co)Se_2/NiCo-LDH core/shell structural electrode with the cactus-like (Ni,Co)Se_2 core for asymmetric supercapacitors. Small, 2018, 15: 1803895
9 Liang M, Zhao M, Wang H, *et al.* Enhanced cycling stability of hierarchical $NiCo_2S_4$@$Ni(OH)_2$@PPy core–shell nanotube arrays for aqueous asymmetric supercapacitors. J Mater Chem A, 2018, 6: 2482–2493
10 Mohamed SG, Hussain I, Shim JJ. One-step synthesis of hollow C-$NiCo_2S_4$ nanostructures for high-performance supercapacitor electrodes. Nanoscale, 2018, 10: 6620–6628
11 Zhang L, Dong L, Li M, *et al.* Ultra-high-rate, ultra-long-life asymmetric supercapacitors based on few-crystalline, porous $NiCo_2O_4$ nanosheet composites. J Mater Chem A, 2018, 6: 1412–1422
12 Zhang Y, Wang B, Liu F, *et al.* Full synergistic contribution of electrodeposited three-dimensional $NiCo_2O_4$@MnO_2 nanosheet networks electrode for asymmetric supercapacitors. Nano Energy, 2016, 27: 627–637
13 Kim SI, Lee JS, Ahn HJ, *et al.* Facile route to an efficient NiO supercapacitor with a three-dimensional nanonetwork morphology. ACS Appl Mater Interfaces, 2013, 5: 1596–1603
14 Chen H, Yang D, Zhang Q, *et al.* A series of MAX phases with MA-triangular-prism bilayers and elastic properties. Angew Chem Int Ed, 2019, 58: 4576–4580
15 Chhowalla M, Shin HS, Eda G, *et al.* The chemistry of two-dimensional layered transition metal dichalcogenide nanosheets. Nat Chem, 2013, 5: 263–275
16 Eftekhari A. The rise of lithium–selenium batteries. Sustain Energy Fuels, 2017, 1: 14–29
17 Yang P, Wu Z, Jiang Y, *et al.* Fractal $(Ni_xCo_{1-x})_9Se_8$ nanodendrite arrays with highly exposed $(01\bar{1})$ surface for wearable, all-solid-state supercapacitor. Adv Energy Mater, 2018, 8: 1801392
18 Shi X, Key J, Ji S, *et al.* $Ni(OH)_2$ nanoflakes supported on 3D Ni_3Se_2 nanowire array as highly efficient electrodes for asymmetric supercapacitor and Ni/MH battery. Small, 2019, 15: 1802861
19 Shi X, Wang H, Kannan P, *et al.* Rich-grain-boundary of Ni_3Se_2 nanowire arrays as multifunctional electrode for electrochemical energy storage and conversion applications. J Mater Chem A, 2019, 7: 3344–3352
20 Song X, Huang C, Qin Y, *et al.* Hierarchical hollow, sea-urchin-like and porous $Ni_{0.5}Co_{0.5}Se_2$ as advanced battery material for hybrid supercapacitors. J Mater Chem A, 2018, 6: 16205–16212
21 Lin J, Wang H, Yan Y, *et al.* Core-branched $CoSe_2$/$Ni_{0.85}Se$ nanotube arrays on Ni foam with remarkable electrochemical performance for hybrid supercapacitors. J Mater Chem A, 2018, 6: 19151–19158
22 Shi X, Wang H, Ji S, *et al.* $CoNiSe_2$ nanorods directly grown on Ni foam as advanced cathodes for asymmetric supercapacitors. Chem Eng J, 2019, 364: 320–327
23 Unni SM, Illathvalappil R, Bhange SN, *et al.* Carbon nanohorn-derived graphene nanotubes as a platinum-free fuel cell cathode. ACS Appl Mater Interfaces, 2015, 7: 24256–24264
24 Zhao J, Li Z, Shen T, *et al.* Oxygen-vacancy Bi_2O_3 nanosheet arrays with excellent rate capability and $CoNi_2S_4$ nanoparticles immobilized on N-doped graphene nanotubes as robust electrode materials for high-energy asymmetric supercapacitors. J Mater Chem A, 2019, 7: 7918–7931
25 Tabassum H, Guo W, Meng W, *et al.* Metal-organic frameworks derived cobalt phosphide architecture encapsulated into B/N co-doped graphene nanotubes for all pH value electrochemical hydrogen evolution. Adv Energy Mater, 2017, 7: 1601671
26 Li Q, Xu P, Gao W, *et al.* Graphene/graphene-tube nanocomposites templated from cage-containing metal-organic frameworks for oxygen reduction in Li-O_2 batteries. Adv Mater, 2014, 26: 1378–1386
27 Wang R, Hao Y, Wang Z, *et al.* Large-diameter graphene nano-

tubes synthesized using Ni nanowire templates. Nano Lett, 2010, 10: 4844–4850
28 Bi H, Chen IW, Lin T, *et al.* A new tubular graphene form of a tetrahedrally connected cellular structure. Adv Mater, 2015, 27: 5943–5949
29 Tabassian R, Kim J, Nguyen VH, *et al.* Functionally antagonistic hybrid electrode with hollow tubular graphene mesh and nitrogen-doped crumpled graphene for high-performance ionic soft actuators. Adv Funct Mater, 2018, 28: 1705714
30 Chen LF, Lu Y, Yu L, *et al.* Designed formation of hollow particle-based nitrogen-doped carbon nanofibers for high-performance supercapacitors. Energy Environ Sci, 2017, 10: 1777–1783
31 Wen Y, Rufford TE, Chen X, *et al.* Nitrogen-doped $Ti_3C_2T_x$ MXene electrodes for high-performance supercapacitors. Nano Energy, 2017, 38: 368–376
32 Song G, Li Z, Meng A, *et al.* Large-scale template-free synthesis of N-doped graphene nanotubes and N-doped SiO_2-coated graphene nanotubes: Growth mechanism and field-emission property. J Alloys Compd, 2017, 706: 147–155
33 Wu X, Jiang L, Long C, *et al.* Dual support system ensuring porous Co-Al hydroxide nanosheets with ultrahigh rate performance and high energy density for supercapacitors. Adv Funct Mater, 2015, 25: 1648–1655
34 Ye B, Huang M, Bao Q, *et al.* Construction of NiTe/NiSe composites on Ni foam for high-performance asymmetric supercapacitor. ChemElectroChem, 2018, 5: 507–514
35 Swesi AT, Masud J, Nath M. Nickel selenide as a high-efficiency catalyst for oxygen evolution reaction. Energy Environ Sci, 2016, 9: 1771–1782
36 Sivanantham A, Shanmugam S. Nickel selenide supported on nickel foam as an efficient and durable non-precious electrocatalyst for the alkaline water electrolysis. Appl Catal B-Environ, 2017, 203: 485–493
37 Muralee Gopi CVV, Reddy AE, Kim HJ. Wearable superhigh energy density supercapacitors using a hierarchical ternary metal selenide composite of $CoNiSe_2$ microspheres decorated with $CoFe_2Se_4$ nanorods. J Mater Chem A, 2018, 6: 7439–7448
38 Ma Q, Yao Y, Yan M, *et al.* Effective enhancement of electrochemical energy storage of cobalt-based nanocrystals by hybridization with nitrogen-doped carbon nanocages. Sci China Mater, 2019, 62: 1393–1402
39 Li R, Wang S, Wang J, *et al.* Ni_3S_2@CoS core–shell nano-triangular pyramid arrays on Ni foam for high-performance supercapacitors. Phys Chem Chem Phys, 2015, 17: 16434–16442
40 Hu W, Chen R, Xie W, *et al.* $CoNi_2S_4$ nanosheet arrays supported on nickel foams with ultrahigh capacitance for aqueous asymmetric supercapacitor applications. ACS Appl Mater Interfaces, 2014, 6: 19318–19326
41 Wang C, Qu H, Peng T, *et al.* Large scale α-$Co(OH)_2$ needle arrays grown on carbon nanotube foams as free standing electrodes for supercapacitors. Electrochim Acta, 2016, 191: 133–141
42 Gao YP, Huang KJ, Wu X, *et al.* MoS_2 nanosheets assembling three-dimensional nanospheres for enhanced-performance supercapacitor. J Alloys Compd, 2018, 741: 174–181
43 Yu W, Lin W, Shao X, *et al.* High performance supercapacitor based on Ni_3S_2/carbon nanofibers and carbon nanofibers electrodes derived from bacterial cellulose. J Power Sources, 2014, 272: 137–143
44 Mei J, Fu W, Zhang Z, *et al.* Vertically-aligned Co_3O_4 nanowires interconnected with $Co(OH)_2$ nanosheets as supercapacitor electrode. Energy, 2017, 139: 1153–1158

Acknowledgements The work was supported by the National Natural Science Foundation of China (51672144, 51572137 and 51702181), the Natural Science Foundation of Shandong Province (ZR2017BB013 and ZR2019BEM042), Higher Educational Science and Technology Program of Shandong Province (J17KA014, J18KA001 and J18KA033), Taishan Scholars Program of Shandong Province (ts201511034), and Overseas Taishan Scholars Program.

Author contributions Meng A, Zhao J and Li Z designed the project and the experiments. Shen T and Huang T performed the experiments. Song G and Tan S performed the products characterizations. Meng A wrote the paper with support from Zhao J and Li Z. All authors contributed to the general discussion.

Conflict of interest The authors declare no conflict of interest.

Supplementary information Supporting data are available in the online version of the paper.

Alan Meng is a professor in the College of Chemistry and Molecular Engineering at Qingdao University of Science & Technology. Her main research interest is on the development of new electrode nanomaterials for energy storage devices including supercapacitors and batteries.

Jian Zhao received his PhD degree from Qingdao University of Science & Technology in 2017. His research interests include the synthesis, characterization, electrochemical performances and mechanism of electrode materials for supercapacitors.

具有高倍率特性和超长循环稳定性的$NiCoSe_2$/Ni_3Se_2片层状阵列修饰N掺杂石墨烯管用于非对称超级电容器

孟阿兰[1], 申童[1], 黄天琪[1], 宋冠英[2], 李镇江[2], 谭淑琴[3], 赵健[2*]

摘要 本文采用一步电沉积法在N掺杂石墨烯纳米管(N-GNTs)上直接生长$NiCoSe_2$/Ni_3Se_2片层状阵列($NiCoSe_2$/Ni_3Se_2-LAs), 并将其作为非对称超级电容器的正极材料. 由于活性材料和骨架之间的协同作用, 在电流密度为1 A g^{-1}的情况下, 构建出的N-GNTs@Ni-$CoSe_2$/Ni_3Se_2-LAs呈现出约1308 F g^{-1}的质量比电容. 更重要的是, 此复合电极材料还显示出优异的倍率性能(100 A g^{-1}下的比电容约为1000 F g^{-1})和超长的循环稳定性(10000次循环后其比电容仍保持为原比电容的~103.2%). 此外, 以N-GNTs@$NiCoSe_2$/Ni_3Se_2-LAs和活性炭(AC)分别为正极和负极组装了一种非对称的超级电容器, 其在2.6 kW kg^{-1}下的能量密度为42.8 W h kg^{-1}, 且具有突出的循环稳定性(10000次循环后其比电容仍保持为原比电容的~94.4%). 因此, 我们的制备技术和新的见解不仅能拓宽多组分复合电极材料的设计, 而且还能促进新型过渡金属硒化物在新一代高性能超级电容器中的实际应用.

